cogent engineering

Cogent Engineering

Taylor & Francis
Taylor & Francis Group

ISSN: (Print) 2331-1916 (Online) Journal homepage: https://www.tandfonline.com/loi/oaen20

Photocatalytic degradation of fractionated crude oil: potential application in oil spill remediation

Benjamin Agyei-Tuffour, Selassie Gbogbo, David Dodoo-Arhin, Lucas N.W. Damoah, Johnson K. Efavi, Abu Yaya & Emmanuel Nyankson |

To cite this article: Benjamin Agyei-Tuffour, Selassie Gbogbo, David Dodoo-Arhin, Lucas N.W. Damoah, Johnson K. Efavi, Abu Yaya & Emmanuel Nyankson | (2020) Photocatalytic degradation of fractionated crude oil: potential application in oil spill remediation, Cogent Engineering, 7:1, 1744944

To link to this article: https://doi.org/10.1080/23311916.2020.1744944

Published online: 07 Apr 2020.

cogent engineering

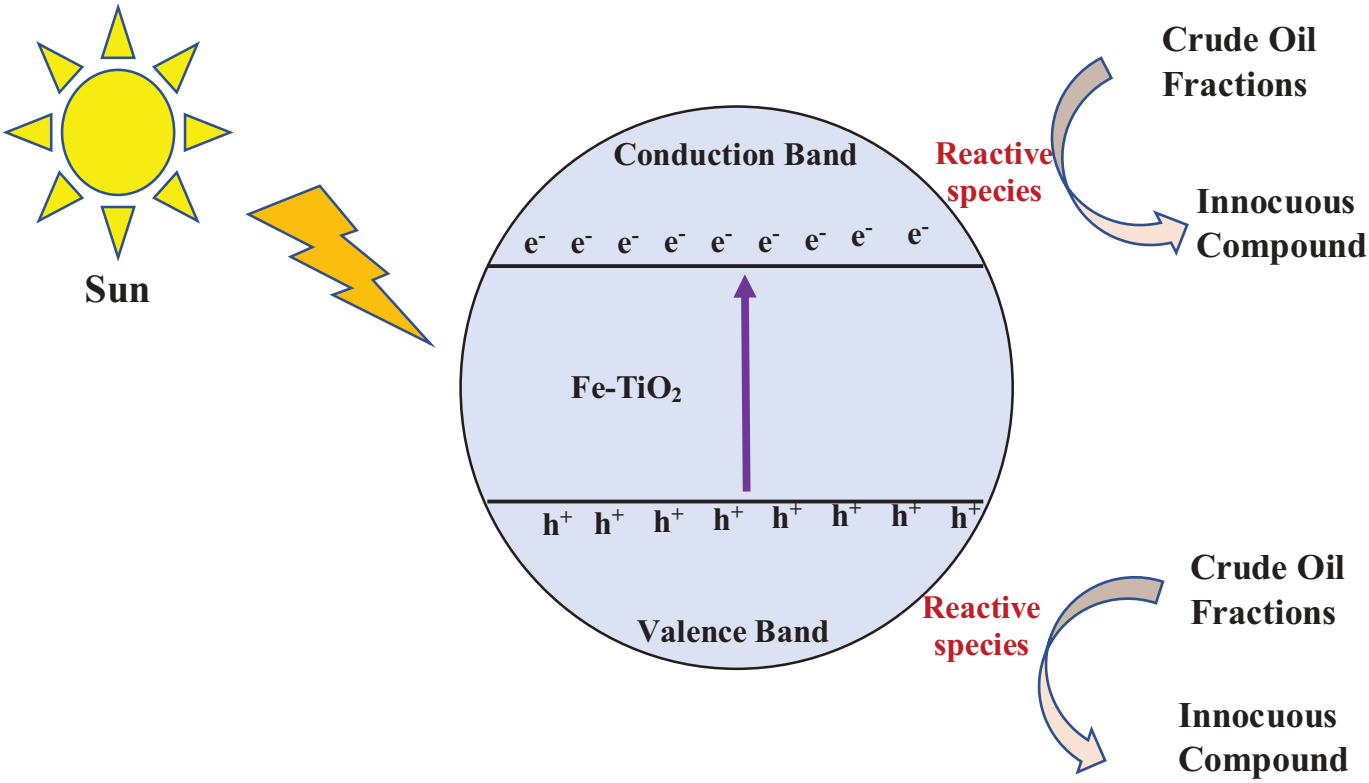

MATERIALS ENGINEERING | RESEARCH ARTICLE

Photocatalytic degradation of fractionated crude oil: potential application in oil spill remediation

Benjamin Agyei-Tuffour, Selassie Gbogbo, David Dodoo-Arhin, Lucas N.W. Damoah, Johnson K. Efavi, Abu Yaya and Emmanuel Nyankson

Cogent Engineering (2020), 7: 1744944

cogent oa

cogent engineering

MATERIALS ENGINEERING | RESEARCH ARTICLE

Photocatalytic degradation of fractionated crude oil: potential application in oil spill remediation

Benjamin Agyei-Tuffour[1], Selassie Gbogbo[1], David Dodoo-Arhin[1], Lucas N.W. Damoah[1], Johnson K. Efavi[1], Abu Yaya[1] and Emmanuel Nyankson[1*]

Received: 11 September 2019
Accepted: 07 March 2020

*Corresponding author: Emmanuel Nyankson, Department of Materials Science and Engineering, University of Ghana, P.O. BOX LG 77, Legon-Accra, Ghana
E-mail: enyankson@ug.edu.gh

Reviewing editor:
Harvey Arellano-Garcia, Brandenburgische Technische Universitat Cottbus-Senftenberg, Germany

Additional information is available at the end of the article

Abstract: The current oil spill remediation strategies are costly and may be toxic to aquatic species and clean-up workers. There is, therefore, the need to look for alternative oil spill remediation strategies that are less costly and non-toxic. This paper presents the potential of TiO_2 and its modified form (Fe-TiO_2) to remediate crude oil fractions under the irradiation of sunlight (UV-Vis), visible (Vis) and ultra-violet (UV) lights. The TiO_2 and Fe-TiO_2 were synthesized by mild hydrothermal method and characterized with X-ray diffraction (XRD), Ultra-violet-visible spectroscopy (UV-Vis), Diffusion reflectance spectroscopy (DRS), Thermogravimetric analysis (TGA), Differential Scanning Calorimetry (DSC), and Scanning Electron Microscopy-Energy Dispersive Spectroscopy (SEM-EDX). The DRS result of Fe-TiO_2 showed an enhanced absorption in the visible light region. The estimated optical band gaps were ~3.12 and ~2.9 eV for TiO_2 and Fe-TiO_2, respectively. The potential application of TiO_2 and Fe-TiO_2 in oil spill remediation was investigated through photocatalytic degradation of benzene soluble fraction, n-hexane soluble fraction and 1:1 volume by volume methanol/benzene soluble fraction in crude oil. The degraded crude oil fractions were characterized with UV-vis, Fourier Transform Infrared (FTIR) Spectroscopy and Gas Chromatography-Mass Spectrometer (GC-MS). The FTIR and UV-vis results showed that the Fe-TiO_2 was more effective in photo-degrading the crude oil fractions under sunlight light irradiation than TiO_2. The GC-MS results showed excellent photodegradation of the various crude oil fractions with the formation of new intermediate products. The results from the study show the potential application of TiO_2 and Fe-TiO_2 in crude oil spills remediation.

Subjects: Materials Science; Chemical Engineering; Environmental

Keywords: TiO_2; Fe-TiO_2; oil spills; crude oil fractions; photocatalysis

PUBLIC INTEREST STATEMENT

Oil spills have devastating effect on the environment. As a result, different strategies are used to minimise their effect on the environment when they occur. The current remediating strategies such as chemical dispersant application and in-situ burning are expensive and have detrimental effect on the environment. In addition, degradation by seawater bacteria is ineffective in remediating water-soluble components of crude oil. This paper investigates into the development of a cost-effective oil spill remediation method using highly abundant solar energy and photocatalysts (TiO_2 and Fe-TiO_2). In the presence of water, photocatalysts upon irradiation with solar energy creates reactive species (radicals) which can attack and break down crude oil fractions into innocuous compounds. This paper reports that Fe-TiO_2 photocatalysis is more effective in degrading/remediating water-soluble components of crude oil under sunlight irradiation when compared to crude oil fractions that are less soluble in water.

1. Introduction

An oil spill is defined as a discrete event in which oil is discharged through neglect, by accident, or with intent over a relatively short time (Etkin, 2001). Oil spills that mostly take place in the marine environment have a ripple effect on the economy. When marine life is affected, there are damaging consequences on the economy, nutrition, health, and many more. As an example, the standard of living of the fisher folks is affected whenever there is an oil spill since it may result in the reduction of household income. Again, the shorelines of the marine environment which serve as recreation centers and tourist sites are destroyed by oil spills (Nyankson, Rodene et al., 2016). In addition, permanent loss of marsh areas may also be observed. The effect of all these is that the importance of the oil industry to the economy is not fully achieved.

Therefore, the need to minimize the occurrence and effects of oil spills on the environment cannot be overemphasized. Chemical dispersants, mechanical containments and collection, in *situ*burning of contained oil on the seas, the use of biological agents to aid degradation and the use of sorbent materials are some of the commonly adopted oil spill remediation techniques. Though significant reduction of the effect of oil spills on the environment has been achieved through these remediation techniques, there are teething problems with many of the existing remediation strategies. For instance, chemical dispersants have been reported to be relatively expensive and toxic to the environment and clean-up workers (Nyankson, Rodene et al., 2016). To reduce the toxicity of chemical dispersants, Nyankson et al. formulated biodegradable, plant based and non-toxic dispersant using soybean lecithin (Efavi et al., 2017; Nyankson, DeCuir et al., 2015; Nyankson, Demir et al., 2016). In addition, other researchers have resorted to the use of naturally occurring halloysite nanotubes and crude oil soluble paraffins as vehicles for dispersant formulations (Nyankson, 2015; Nyankson et al., 2014; Nyankson, Olasehinde et al., 2015; Owoseni et al., 2014, 2016).

The application of chemical dispersant results in the reduction of the surface energy between the oil slick and water, and when enough energy is applied to the oil-water-dispersant mixture, the oil is broken down into smaller droplets that diffuse vertically and horizontally in the ocean column. Bacteria in the sea then feed on the oil droplets. However, many years after the Gulf of Mexico oil spill, researchers have reported that, the water-soluble component of the spilled oil are still present in the Gulf of Mexico (Ziervogel et al., 2012). On the other hand, it has been reported that paraffins are easily degraded through biodegradation. The various fractions of crude oil therefore respond differently to biodegradation. Therefore, a remediation strategy that is effective in degrading all the components in crude oil must be developed.

After the occurrence of oil spills, some of the spilled crude oil are lost through photooxidation. This loss though photooxidation has been observed to be preeminent in crude oils with high water-soluble fractions (Lehr, 2001). This photooxidation may be enhanced through the introduction of photocatalysts such as TiO_2(Dodoo-Arhin et al., 2018). The authors of this paper have examined how the various fractions of crude oil will respond to photocatalysis. The results from this study will be essential in deciding whether photocatalysis can be used as a stand-alone oil spill remediation technique or be added to existing techniques to enhance their efficiency. Photocatalysis is the acceleration of a photoreaction in the presence of a catalyst. When a photocatalyst (e.g., TiO_2) is irradiated with a light source, photons with energy greater than or equal to the band gap of the photocatalyst is absorbed. This results in the excitation of electrons from the valence band to the conduction band creating an electron hole pair. The valence band is strongly oxidizing while the conduction band is strongly reducing. The valence band hole and the conduction band electrons can attack water molecules and dissolved oxygen resulting in the creation of reactive oxygen species (ROS). ROS can attack pollutants and degrade them into innocuous compounds. Photocatalysis has been reported to be an effective way of degrading water-soluble pollutants such as dyes, pesticides and pharmaceuticals (Hoffmann et al., 1995; Nyankson, Agyei-Tuffour, Adjasoo et al., 2019; Nyankson, Agyei-Tuffour, Annan et al., 2019; Nyankson & Kumar, 2019). Since crude oil is made up of different organic components, it is hypothesized that photocatalysis can be used to photodegrade the various organic fractions present in crude oil resulting in an effective remediation.

Common photocatalysts such as Ag_3PO_4, ZnO, SnO_2, ZrO_2, TiO_2, and CuO are effective in the photodegradation of different compounds (Agbe et al., 2019). Among these photocatalysts, TiO_2 possesses greater potential to photodegrade organic pollutants due to its desirable characteristics such as high chemical and thermal stability, tunable band gap and availability in greater quantities (Ajaj, 2015; Chong et al., 2010; Fujishima et al., 2000; Fujishima & Zhang, 2006; Fujishima et al., 2007; Gaya & Abdullah, 2008; Herrmann, 1999; Huang et al., 2016; Mills & Le Hunte, 1997; Nasiri et al., 2018; Santos et al., 2012). Photochemical degradation of polycyclic aromatic hydrocarbon crude oil films with TiO_2 has been reported and modelled (Lee & Ryan, 1983; Plata et al., 2008). However, the wide band gap of TiO_2 (~3.2 eV) limits its application to the UV region of the electromagnetic spectrum. The practical application of TiO_2 photocatalysts is limited since only 4% of the solar radiation that arrives on the earth's surface is UV (Martin et al., 2015; Murphy et al., 2006). When modified through doping or by creating a heterojunction, the optical properties of TiO_2 are enhanced and therefore able to absorb radiations in both ultraviolet and visible light regions of the electromagnetic spectrum. This improves the photoabsorbance and consequently the photodegradation of pollutants (Ajaj, 2015; Huang et al., 2016). The performance of TiO_2 has been enhanced by coupling it with other semiconductors such as Ag_3PO_4 (Lu et al., 2015), and by decorating with either Ag (Coto et al., 2017) or Fe (Fàbrega et al., 2010). Fe is mostly employed for modification of TiO_2 due to its unique half-filled electronic configuration (C.-y. Wang et al., 2000) and its relatively cheaper cost when compared to Ag. The unique half-filled electronic configuration may narrow the energy band gap and also reduce the electron-hole recombination (Meng et al., 2013).

The authors are not aware of any photocatalytic degradation of crude oils from the recently discovered Jubilee and TEN fields in the South Western part of Ghana. The TEN and Jubilee oil fields are shown in Figure 1. Hence, in this work, TiO_2 and Fe-TiO_2 were synthesized by mild hydrothermal method and characterized. Crude oil from the Jubilee and TEN Fields in Ghana was fractionated into benzene (B SF), n-hexane (n-H SF) and 1:1 volume by volume benzene/methanol (1: v/v M:B SF) soluble fractions. The pristine and modified TiO_2 were contacted with crude oil fractions under the irradiation of visible light (vis), ultraviolet light (UV) and sunlight (UV-vis). The extent of the degradation was examined by UV-vis spectrophotometry and FTIR while the photoproducts were identified with GC/MS. The implications of the results are discussed to ascertain the potential of TiO_2 and Fe-TiO_2 as reliable catalysts in crude oil photodegradation.

This article includes Introduction, Materials and Methods, Results and Discussion and Conclusion.

2. Materials and methods

2.1. Materials

Isopropanol (IPA), Titanium tetraisopropoxide (TTIP), Dichloromethane (DCM), Benzene, n-Hexane, Acetone and the Methanol were purchased from Sigma Aldrich, USA., Ethanol was purchased from Fisher Scientific, UK., Hydrochloric acid (HCl) from Analar, England, and Crude oil was obtained from Tullow Oil Ghana.

A summary of the research methodology is presented in the flowchart in Figure 2.

2.2. Synthesis of TiO_2, Fe-TiO_2 nanoparticles

Mild hydrothermal method was used to synthesize the TiO_2 and Fe-TiO_2 nanoparticles. In a typical synthesis of TiO_2 nanoparticles, TTIP and isopropanol were mixed in a volume ratio of 1:10 and named solution A. Solution B which is made up of hydrochloric acid (HCl) and water (H_2O) in a 1:10 volume ratio was also prepared. Solutions A and B were mixed and subjected to rigorous stirring at 1200 rpm for 24 h to form a milky solution. The resultant mixture was then centrifuged at 1800 rpm for 15 min and washed several times with deionised water. The solid particles collected after centrifugation were dispersed in a solution made up of 60 mL of water and 60 mL of ethanol and autoclaved at 115 °C for 8 h. The autoclaved particles were dried in an oven at 70 °C for 48 h. The as-prepared powder was then crushed and sieved with 75 µm sieve to obtain the TiO_2 particles.

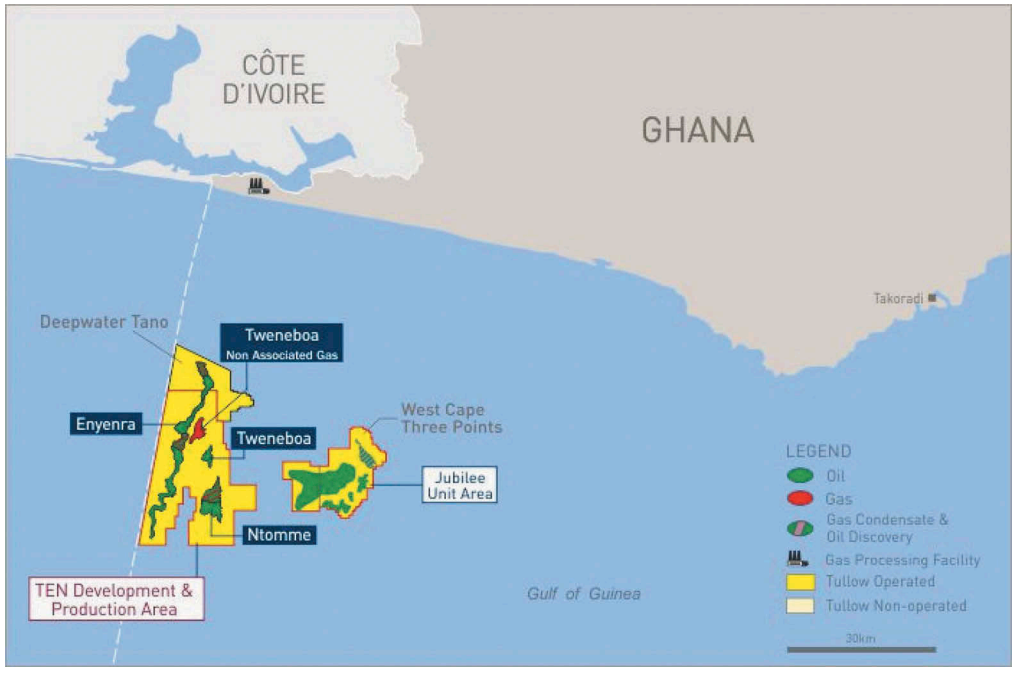

Figure 1. The jubilee and TEN (*Tweneboa Enyenra Ntomme*) oil fields (Ghana, 2018).

A similar procedure was used for the synthesis of the Fe-TiO_2 particles. However, 88 mg of $FeCl_3.6H_2O$ was added to the resultant solution obtained by mixing solutions A and B.

2.3. Characterization of TiO_2 and Fe-TiO_2

The structure, morphology, optical and thermal properties of the as-prepared TiO_2 and Fe-TiO_2 particles were characterized using X-ray diffraction (XRD), scanning electron microscopy (SEM), energy-dispersive X-ray spectroscopy (EDX), diffuse reflectance spectroscopy (DRS), thermogravimetric analysis (TGA), and differential scanning calorimetry (DSC).

2.3.1. Microstructural characterization of Fe-TiO_2 and TiO_2

The phases present and the microstructure of the TiO_2 and Fe-TiO_2 particles were identified using X-ray powder diffraction (XRD) patterns. The XRD characterization was done using a Bruker D8 x-ray diffractometer in theta-theta configuration with anode material Cu K-Alpha1 (wavelength of 1.54060 Å) and generator settings (40 mA, 45 kV). The XRD patterns of all the randomly oriented

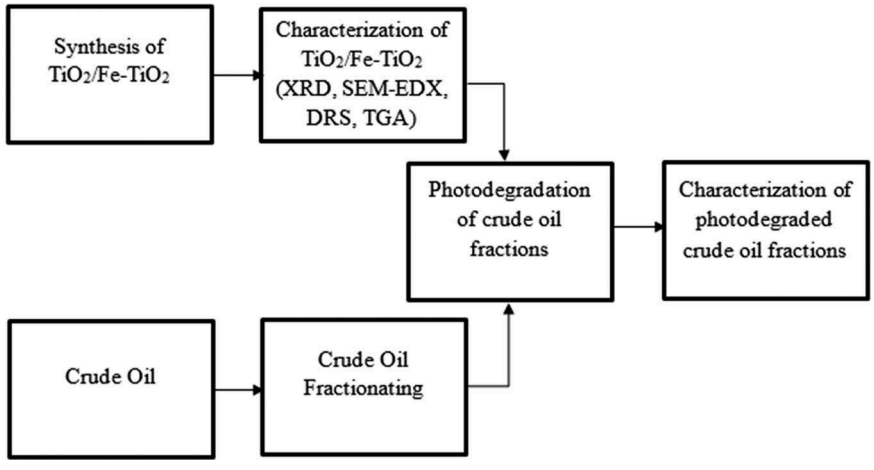

Figure 2. Flowchart of the research methodology.

powder specimens were recorded in the 2θ range of 20°- 70° with a step size of 0.017°. The Debye Scherrer's equation was used to compute the crystallite sizes of the TiO_2 and the Fe-TiO_2.

The morphology and the chemical composition of the prepared nanoparticles were examined using a FEI Nova NanoSEM 450 scanning electron microscope fitted with an EDX acquisition detector, operated at an acceleration voltage of 5 kV and an aperture size of 30 µm. The prepared samples were mounted on stainless steel stubs by the help of an adhesive tape and sputter coated with a thin layer of platinum metal.

2.3.2. Optical and thermal characterization of TiO_2 and Fe-TiO_2

The Vertex 70 v (Bruker) Fourier Transform Infrared (FTIR) spectrometer was used to record the FTIR spectra in transmission mode. The spectra were measured within a wavenumber range of 4000–400 cm^{-1} with 4 cm^{-1} resolution. The recorded spectra data was analysed using the Opus software.

Diffuse reflectance spectroscopy (DRS) was carried out using a UV-vis spectrometer. The Kubelka Munk function (Kubelka & Munk, 1931; Morales et al., 2007) was then used to compute the optical band gap of the TiO_2 and the Fe-TiO_2.

The thermal stability behavior (TG-DTA) of the nanoparticles were analysed on a TA Instrument Q500 thermal analyzer. The Analysis was performed using air at a heating rate of 10°C min^{-1}.

2.4. Fractionating of crude oil sample

The crude oil was separated into three fractions. The fractionating was done by adding 50 mL of crude oil to 181 g silica gel in a chromatographic column. Five hundred milliliters of n—hexane was first added to the crude oil in the column to elute the n-hexane soluble fraction. Secondly, 500 mL of Benzene was also added to the residual crude in the column for the elution of the benzene soluble fraction. Lastly, a solution of 250 mL of methanol and 250 mL of Benzene was again added to the residual crude after the second elution, to elute the 1:1 methanol-benzene soluble fraction. The eluate samples were concentrated by evaporating the solvent-crude oil fractions mixture using the rotary evaporator at 40°C.

2.5. Photodegradation of crude oil fractions

0.2 mL of the crude oil fraction was measured and added to 50 mL of deionised water in a 200 mL beaker. Fifty milligrams of the photocatalyst was added to the mixture of the crude oil fraction and the deionised water. The resultant mixture was placed in the light source (UV or visible) chamber. In the case of using sunlight as the light source, the crude oil-water-photocatalyst mixture was placed in the sun. Continuous stirring at 350 rpm was done to ensure that the photocatalyst mixes well with the water and crude oil. Irradiation was done continuously for 4 h after which 7 mL of dichloromethane was added to the resultant mixture to extract the degraded crude oil. The dichloromethane (DCM) with the dissolved degraded crude oil (or crude oil fraction) was separated from the photocatalyst and water using separation funnel. The dissolved oil was further centrifuged at 600 rpm for 15 min to ensure that all residual photocatalysts were removed. The extracted crude oil in DCM was characterized using UV-Vis, FTIR and GC/MS.

2.6. FT-IR, UV-Vis spectrophotometry and gas chromatography-mass spectrometry (GC/MS) analysis of degraded crude oil fractions

The Vertex 70v (Bruker) was used to obtain the transmission FTIR spectra of the photodegraded and undegraded crude oil fractions. Genesys ^{TM} 10 UV-Vis spectrophotometry was used to examine the extent of photodegradation.

The combined processes of Gas Chromatography and Mass Spectrometry have been used for effective chemical analysis. The two when used together can help to make conclusive identification of compounds (Douglas, 2004). The GC component used for the analyses was PerkinElmer Clarus 580 and the MS was PerkinElmer Clarus SQ 8S. These were the GC/MS conditions

employed; the oven initial temperature was 80°C for 0 min, ramped at 10°C min^{-1} to 240°C, and then held for 2 min. The temperature was then ramped to 280 °C at 5°C min^{-1}, and then held at 280 °C for 10 min. The injection temperature and volume were 250 °C and 1 µL, respectively. The split ratio was 20:1. The carrier gas used was He while the solvent delay time was 2.50 min. The transfer and source temperatures were 250 °C and 150 °C, respectively. Scanning was done from 50 to 500 Da and the column dimension was 27.0 m x 250 µm.

3. Result and discussion

3.1. Microstructural and optical characterization of TiO_2 and Fe-TiO_2

Figure 3 shows the XRD patterns of pure TiO_2 and Fe-TiO_2 powders. The observed XRD peaks confirmed the formation of anatase TiO_2 (JCPDS No. 21–1272). The intensity of the Fe-TiO_2 peaks is slightly weaker than that of the pure TiO_2. The peaks for the Fe-TiO_2 also shifted slightly to higher 2θ values. These observations can be attributed to the presence of the Fe^{3+} in the structure of the TiO_2. From the XRD spectrum of TiO_2 and Fe-TiO_2 in Figure 2, the anatase phase of TiO_2 was the only observed phase in the XRD spectrum for TiO_2 and its peaks (101), (004), (200), (105) and (204) were quite wide and not sharp. This is indicative of incomplete crystallization due it amorphous component (Ba-Abbad et al., 2012; Jing et al., 2001; Xu et al., 1999). The amorphous phase present in the anatase phase of the TiO_2 plays an important role in the photocatalytic process (Yoon & Cocke, 1986). The anatase phase of TiO_2 is admitted to be the best active phase for photodegradation of organic materials. This is because it is formed at lower temperatures which make it crystallite sizes smaller than that of the rutile which is formed at higher temperatures (>500 °C). This gives the anatase phase high surface area. A large surface area enables the anatase phase to adsorb more of the organic materials for photocatalysis (Chong et al., 2010) due to large number of active sites. It should however be noted that, an additional peak was observed in the XRD spectrum for Fe-TiO_2. The additional peak may be attributed to the presence of Fe_2O_3 which may have been formed from the oxidation of the Fe used in the synthesis.

Due to the fact that the photocatalytic activity is dependent on the active sites which is also influenced by the crystallite size, the Debye-Scherrer equation (equation 1) was used to compute the crystallite sizes of the Fe-TiO_2 and TiO_2.;

$$d = \frac{\kappa\lambda}{\beta \cos\theta} \tag{1}$$

Where:

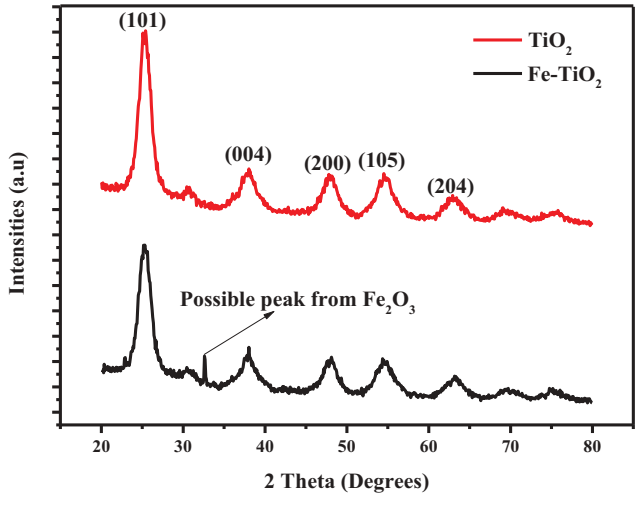

Figure 3. XRD patterns of the undoped and Fe-doped TiO_2 powders.

D is the mean size of the crystallites, κ is the shape factor and a good approximation is 0.9, λ is the X-ray wavelength, β is the full width at half maximum (FWHM) in radians of the X-ray diffraction peak and θ is the Braggs angle (deg.) (Ba-Abbad et al., 2012; Mardare et al., 2000).

From Table 1, it can be seen that the crystallite size of the Fe-TiO_2 is smaller than that of the TiO_2. This is so because the successful addition of the Fe^{3+} reduced the growth rate of the TiO_2 crystallite (Cheng et al., 2018; Deng et al., 2009; Kim et al., 2013). The smaller crystallite sizes of Fe-TiO_2 are expected to enhance its photocatalytic activity.

The optical properties of TiO_2 and Fe-TiO_2 were examined through diffused reflectance spectroscopy (DRS) analysis and the results presented in Figure 4. The reflectance of the TiO_2 shows 100% in the range of 400–800 nm implying TiO_2 does not absorb light in the visible region of the electromagnetic spectrum. On the other hand, Fe-TiO_2 recorded a much lower reflectance in the visible region implying that the TiO_2 became active in the visible light upon the incorporation of Fe. This therefore suggests that Fe-TiO_2 photocatalyst will be more active in the visible light region than TiO_2.

The Kubelka Munk model was used to estimate the optical bandgap of the synthesized TiO_2 and Fe-TiO_2 photocatalysts (Kubelka & Munk, 1931; Morales et al., 2007). The plots derived from the Kubelka Munk model are presented in Figure 5. The optical bandgap values estimated from Figure 5 were ~3.12 and ~2.91 eV for TiO_2 and Fe-TiO_2, respectively. Doping of TiO_2 with Fe^{3+} to form Fe-TiO_2 resulted in the reduction of the band gap from ~3.12 to ~2.91 eV. The enhancement in the visible light absorption of Fe-TiO_2 (in Figure 4) can be attributed to the reduction in its band gap energy. In addition to the Fe^{3+} reducing the band gap energy of TiO_2, the Fe^{3+} may act as electron-trapping sites in the structure of the TiO_2. This will help in reducing the electron-hole recombination and subsequently improve the photocatalytic process.

3.2. Morphological and surface analysis of the TiO_2 and Fe-TiO_2

The surface morphology of TiO_2 and Fe-TiO_2 was examined through Scanning Electron Microscopy (SEM) imaging and the results presented in Figure 6(a, b), respectively. It can be deduced from the

Table 1. Crystallite sizes of the TiO_2 and the Fe-TiO_2 deduced from the crystallographic plane (101)

Sample	Peak Position 2θ(°)	FWHM 2θ(°)	Crystallite Size (nm)
TiO_2	25.3	2.08 ± 0.01	4.10 ± 0.23
Fe-TiO_2	25.3	2.09 ± 0.01	3.85 ± 0.22

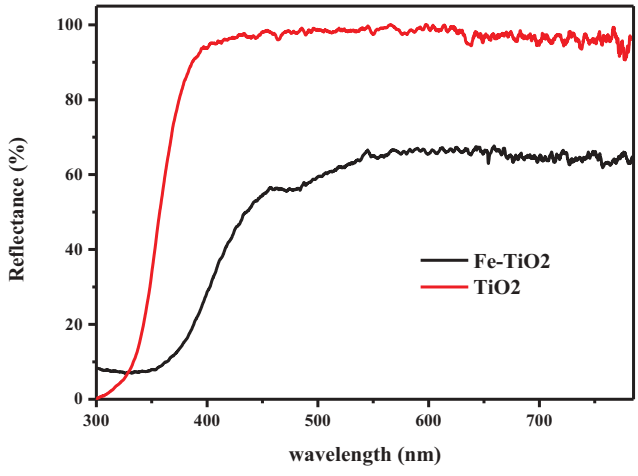

Figure 4. Diffuse Reflectance Spectroscopy (DRS) of the as-prepared TiO_2 and Fe-TiO_2.

SEM images that the sizes of the particles are not uniform (smaller particles are dispersed on the surface of the larger particles) and they appeared in chunks and this can be attributed to the grinding of the samples.

The elemental composition of the TiO_2 and Fe-TiO_2 was analysed with EDX. Figure 5 shows the energy-dispersive X-Rays spectroscopy (EDX) of TiO_2 (Figure 6(a)) and that of Fe-TiO_2 (Figure 6(b)). Figure 6(a) shows peaks for Titanium and Oxygen suggesting the formation of pure TiO_2 without any impurities which agrees with the XRD results. The EDX detected the presence of Fe (ca. 1.13 wt. %) in the Fe-TiO_2 (Figure 6(b)). The wt.% of Fe detected is close to the experimental amount (ca. 1 wt.%). Figure 6(b) shows peaks for Fe, Ti, and O which suggest the TiO_2 was successfully doped with the Fe^{3+} without any impurities forming. This also agrees with the XRD results. The unidentified peaks at 2 keV can be attributed to the Pt that was used for sputter coating the samples before the SEM-EDX analyses.

3.3. Thermal analysis of the as-prepared TiO_2 and Fe-TiO_2

The thermal behaviour of the TiO_2 and the Fe-TiO_2 were examined and the results presented in Figures 7 (DSC) and 8 (TGA). Generally, the thermal behaviour of TiO_2 depends on the chemical composition, preparation condition, and the phases that are present (Tang et al., 2012; Yu et al., 2000). It can be seen in Figure 7 that the DSC results for both TiO_2 and Fe-TiO_2 followed similar patterns and possessed similar features. The first peak which is endothermic at 95°C for TiO_2 and 110°C for the Fe-TiO_2 represent the loss of adsorbed water on the surface corresponding to a weight loss as revealed in Figure 8 (TGA). The second peak observed at a temperature of 350° C for TiO_2 and 400°C for Fe-TiO_2 is exothermic and represent the oxidation and decomposition of the organic substances present. The decomposition also resulted in a mass loss as can be seen in Figure 8. Phase transformation from anatase to the rutile phase occurred above 400°C (Hu et al., 2013; Tang et al., 2012).

From the TGA results presented in Figure 8, three decomposition stages were observed from the curve in both samples. Considering the TiO_2 curve, ca.14% weight loss was observed, and this is due to the elimination of the ethanol and water present in the sample when the temperature increased from 25 °C to 140 °C. The second stage also shows ca. 7% weight loss attributable to the complete decomposition of the organic compounds in the sample as the temperature increased from 140 °C to 443 °C. Taking note of the Fe-TiO_2 curve, the first stage shows ca. 14% weight loss which indicates the elimination of the presence of the ethanol and water present in the sample. The second stage also shows a weight loss of ca. 17% representing the decomposition of all the organic compounds as the temperature increased from 140 °C to 443 °C. In the final stage, there is no weight loss at temperatures > 443 °C. The TGA curve for both samples showed no mass loss

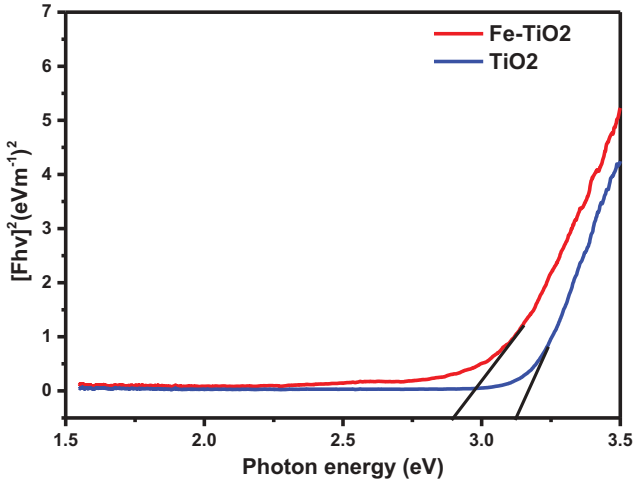

Figure 5. Kubelka Munk transformed reflectance for estimating the optical band-gap energy of TiO_2 and Fe-TiO_2.

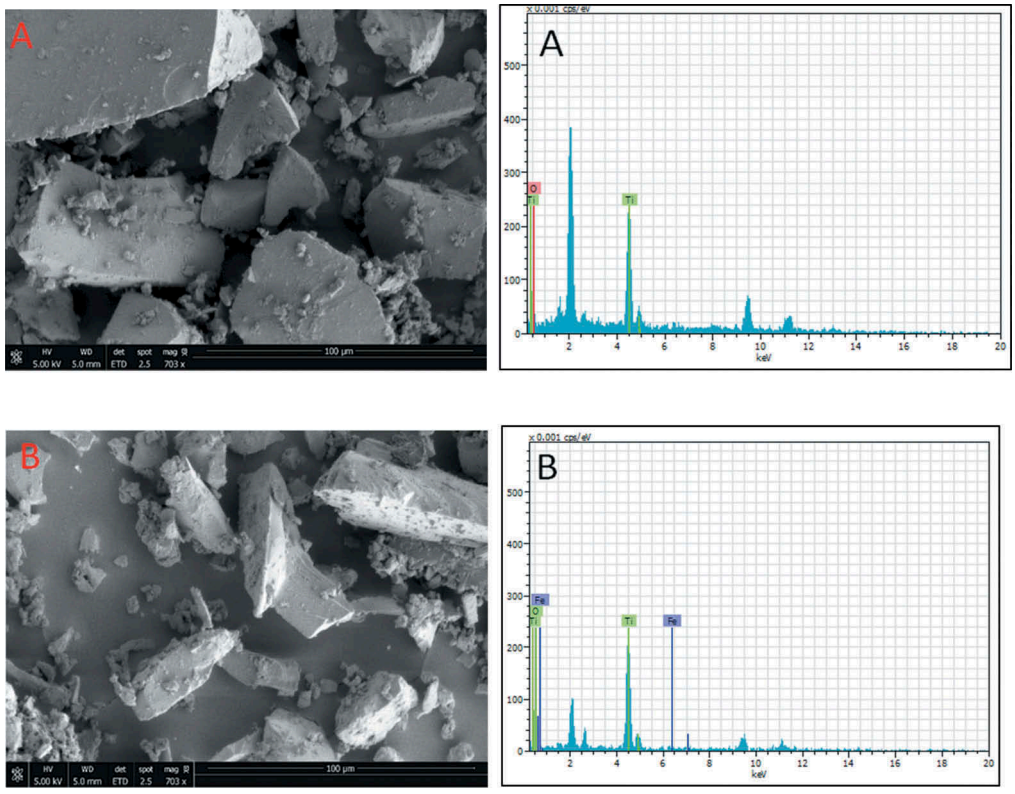

Figure 6. Scanning Electron Micrographs (SEM) with EDS of (a) TiO_2 and (b) Fe-TiO_2, respectively.

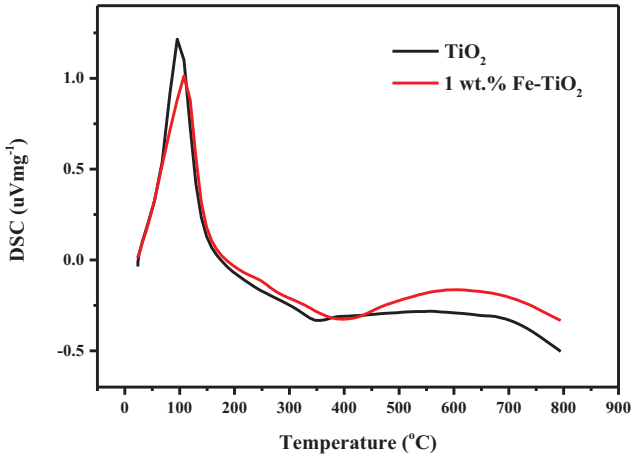

Figure 7. Differential Scanning-Calorimetry (DSC) of the as-prepared TiO_2 and Fe-TiO_2.

after 443 °C suggesting a total decomposition of all organic components in the TiO_2 (Ba-Abbad et al., 2012; J. Wang et al., 2008).

3.4. Fourier Transform Infrared (FTIR) spectroscopy analysis

The FTIR spectra of the synthesized TiO_2 and Fe-TiO_2 photocatalysts are shown in Figure 9. In both the TiO_2 and the Fe-TiO_2 the stretching of the hydroxyl (O-H) bonds occurred between the wavenumbers 3000 to 3500 cm^{-1}. This signifies the presence of moisture in the as-prepared samples. The peaks observed between 1250 and 1750 cm^{-1} band can be attributed to the titanium carboxilate stretching mode emanating from the Titanium Isopropoxide (TTIP) and ethanol as

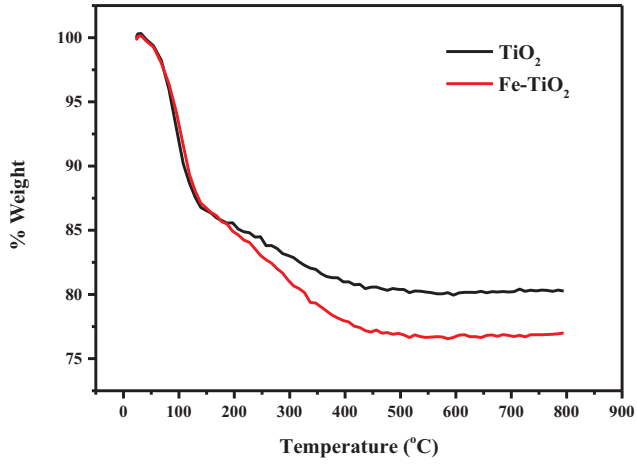

Figure 8. Thermogravimetric Analyses (TGA) of the as-prepared TiO_2 and Fe-TiO_2.

precursors. The peak between ~800 to ~450 cm^{-1} shows the Ti-O functional group indicating the formation of TiO_2 particles (García-Serrano et al., 2009; Zhou et al., 2017).

3.5. Characterization of the degraded crude oil fractions

The degraded and undegraded crude oil fractions were characterized by FTIR, UV-vis spectrophotometry and GC-MS.

3.5.1. FTIR characterization of the fractions of the crude oil

Different researchers have suggested FTIR as a rapid and cost-effective technique for analysing crude oil fractions (Abdulkadir et al., 2016; Akmaz et al., 2011). For all the fractions (benzene soluble, n-hexane soluble and methanol-benzene soluble) used in this study, the FTIR spectra (Figure 10) showed bands at ca. 2900 cm^{-1}, 2850 $cm^{-1,}$ 1500 cm^{-1} and 1350 cm^{-1} due to the presence of CH_2 and CH_3 functional groups (Akmaz et al., 2011). The absorption bands identified at 1600 cm^{-1} and 1700 cm^{-1} can be attributed to C = C and C = O functional groups, respectively. The peaks observed at 675 cm^{-1}, 700 cm^{-1} and 900 cm^{-1} depict aromatic rings (Abdulkadir et al., 2016). The identified absorption bands of the crude oil fractions in Figure 10 have similar features with the FTIR spectra of crude oil fractions reported by other researchers (Akmaz et al., 2011; Ali & Bukhari, 1989; Aske et al., 2001; Buenrostro-Gonzalez et al., 2001; Peralta-Martinez et al., 2008).

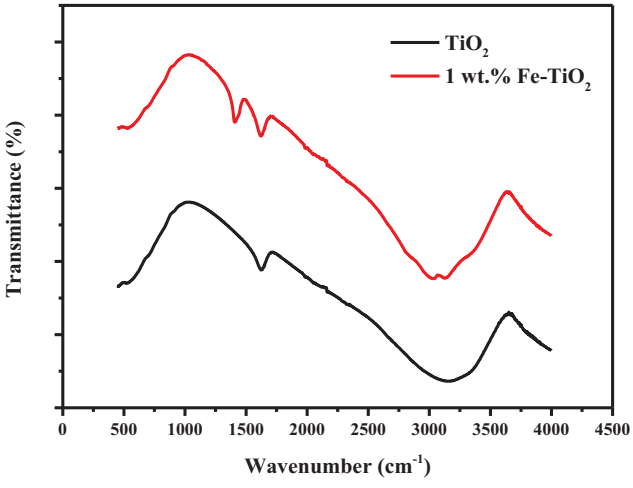

Figure 9. FTIR of TiO_2 and Fe-TiO_2 powders.

Figure 11 shows the FTIR results of the photoproducts of the crude oil fractions after subjecting them to sunlight, visible light and UV light irradiation. Differences can be observed among all the FTIR spectra of the photodegraded products and the undegraded products presented in Figuress 11. That is after the photodegradation, there was the formation and disappearance of functional groups. It was observed from the Figures that the undegraded fractions had bands appearing at around ~2900 cm^{-1}, ~2850 $cm^{-1,}$ ~1500 cm^{-1} and ~1350 cm^{-1} due to CH_2 and CH_3 functional groups (Akmaz et al., 2011). Again absorption bands were identified at 1600 cm^{-1} due to C = C, 1700 cm^{-1} due to C = O and at 675 cm^{-1}, 700 cm^{-1} and 900 cm^{-1} depicting the presence of aromatic rings (Abdulkadir et al., 2016). The differences in the spectra between the undegraded crude oil fractions and the degraded fractions with or without the photocatalyst can be seen in the bands that appeared at wavenumber of ~3,250–3,500 cm^{-1} which is indicative of an O-H or an N-H functional group. Bands also appeared around 1700 cm^{-1} and ca. 470–800 cm^{-1} which indicate C = O and aromatics, respectively. The differences observed suggest that, the photodegradation of the crude oil fractions was successful and hence new intermediate compounds have been formed. However, the presence of the CH_2 and CH_3 functional groups in both the degraded and undegraded crude oil fraction depict that most of the compounds in the degraded and undegraded fractions are paraffins.

3.5.2. UV-Vis spectrophotometry analysis of the crude fractions

UV-vis spectrophotometry can be used to examine the concentration of the fractionated crude oil before and after photodegradation. A decrease in the absorbance after photocatalysis depicts a decrease in concentration of the crude oil fraction. The UV-vis spectrophotometry of the degraded and undegraded crude oil fractions are presented in Figure 12. Generally, Fe-TiO_2 was more efficient in degrading the fractionated crude oil fractions under sunlight and visible light irradiation. On the other hand, the TiO_2 with a bandgap of ~3.12 eV was more efficient in degrading the crude oil fractions under UV light irradiation than the Fe-TiO_2 with a band gap of ~2.9 eV. The trend observed in the UV-vis spectrophotometry analysis is in line with the DRS results. Where the TiO_2 was redundant especially in the visible light, it was seen to be impeding light penetration and so derailing the degradation of the crude oil fractions in the solution (Dong et al., 2010). It also emerged that photodegradation occurred even without the presence of a photocatalyst; however, the presence of the photocatalyst hastened the photodegradation process. This can be seen in Figuress 12 where the crude oil fraction irradiated without a photocatalyst (Nil+ crude oil fractions) showed lower absorbance than the undegraded crude fractions. It has already been reported that, after oil spill occurs, some of the crude oil is lost through photo-oxidation and evaporation. This photo-oxidation and evaporation is dependent on the intensity of sunlight (Ali & Bukhari, 1989; Nyankson, Rodene et al., 2016).

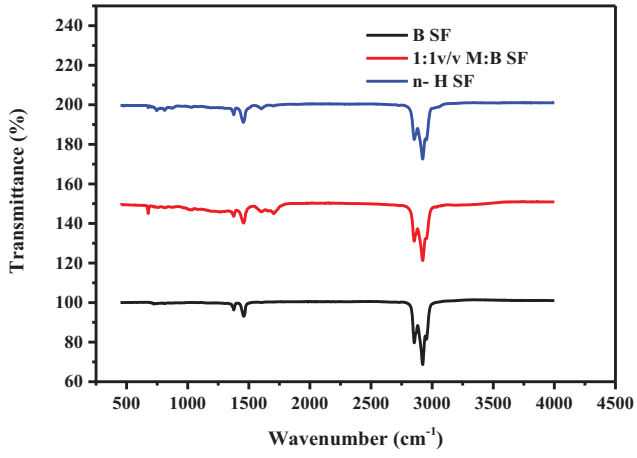

Figure 10. FTIR analysis of the crude oil fractions.

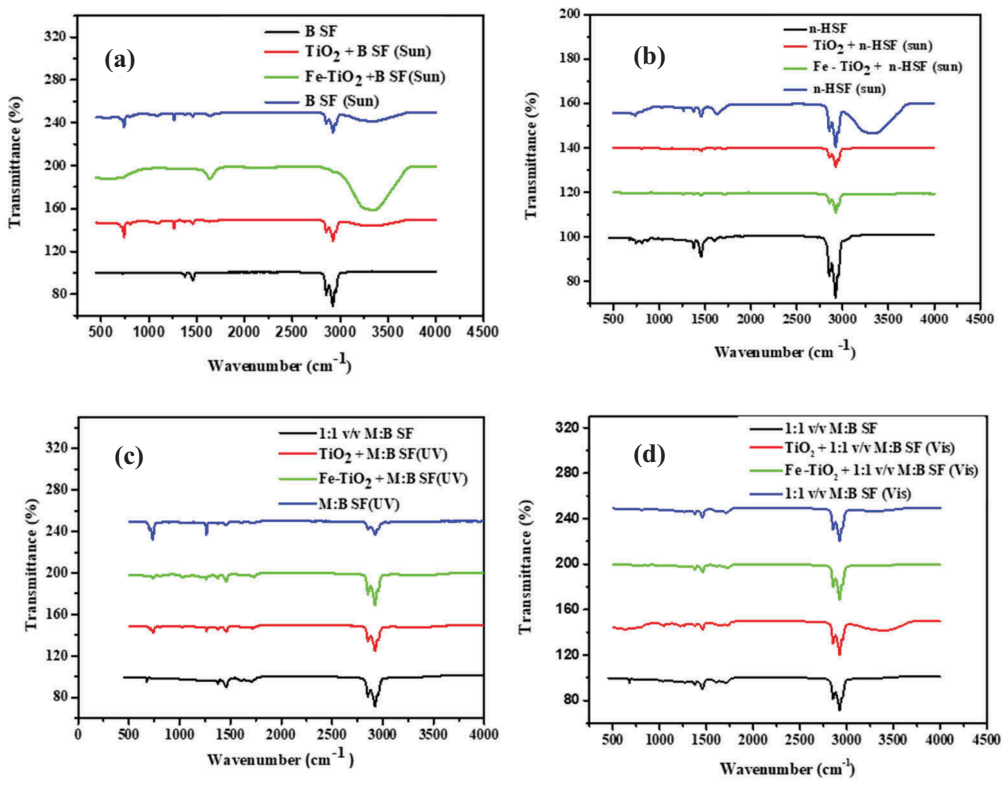

Figure 11. Photocatalytic degradation of (a) Benzene soluble fraction under sunlight irradiation, (b) n-hexane soluble fraction under sunlight irradiation, (c) Methanol-Benzene Soluble Fraction under UV irradiation and (d) Methanol-Benzene soluble fraction under visible light irradiation by TiO_2 and Fe-TiO_2.

The extent of photodegradation varied among the crude oil fractions. For instance, under sunlight irradiation, the photodegradation of the benzene soluble fraction (Figure 12(a)) was more pronounced than the n-hexane and methanol-benzene soluble fractions. The variation can be seen in the dramatic reduction in the concentration of the benzene soluble fraction after photocatalysis. This observation can be attributed to the relatively higher aqueous solubility of the benzene soluble fractions when compared to that of the n-hexane and methanol-benzene soluble crude oil fractions. The aqueous solubility enhanced photocatalytic activity due to proximity of the dissolved fractions to the photocatalyst (TiO_2 or Fe-TiO_2) and the reactive oxygen species generated.

3.5.3. Gas chromatography and mass spectrometry (GC-MS)

The FTIR and UV-vis spectrophotometry analyses confirmed the degradation of the various crude oil fractions by the photocatalysts under visible, sunlight, and UV light irradiations. The photoproducts from the photodegradation of the crude oil fractions which were irradiated under sunlight were analysed qualitatively and identified using the GC-MS.

3.5.3.1. GC-MS analysis of the benzene soluble crude oil fraction after photocatalysis. The GC-MS chromatograms obtained from the photodegradation of the benzene soluble crude oil fraction are presented in Figure 13. It can be seen in Figuress 13(b,c) that most of the peaks disappeared after photodegradation when compared to the undegraded benzene soluble fraction (Figure 13(a)). A hump of unresolved complex mixtures (UCM) which is evident of severe photodegradation of crude oil (Abdulkadir et al., 2016; Ali & Bukhari, 1989) were also observed. Comparing Figuress 12(b,c), and Tables 2 and 3, it can be seen that Fe-TiO_2 degraded most of the benzene soluble fraction of the crude oil, showing more diminished concentration of compounds, disappearance of existing compounds and the appearance of UCM's peaks which indicate severe degradation than the fraction degraded using TiO_2. This observation is also evident in the FTIR and the UV-Vis spectra presented. New compounds emerged from the photodegradation of the benzene soluble fraction as evidenced in Tables 2 and 3. There was the disappearance

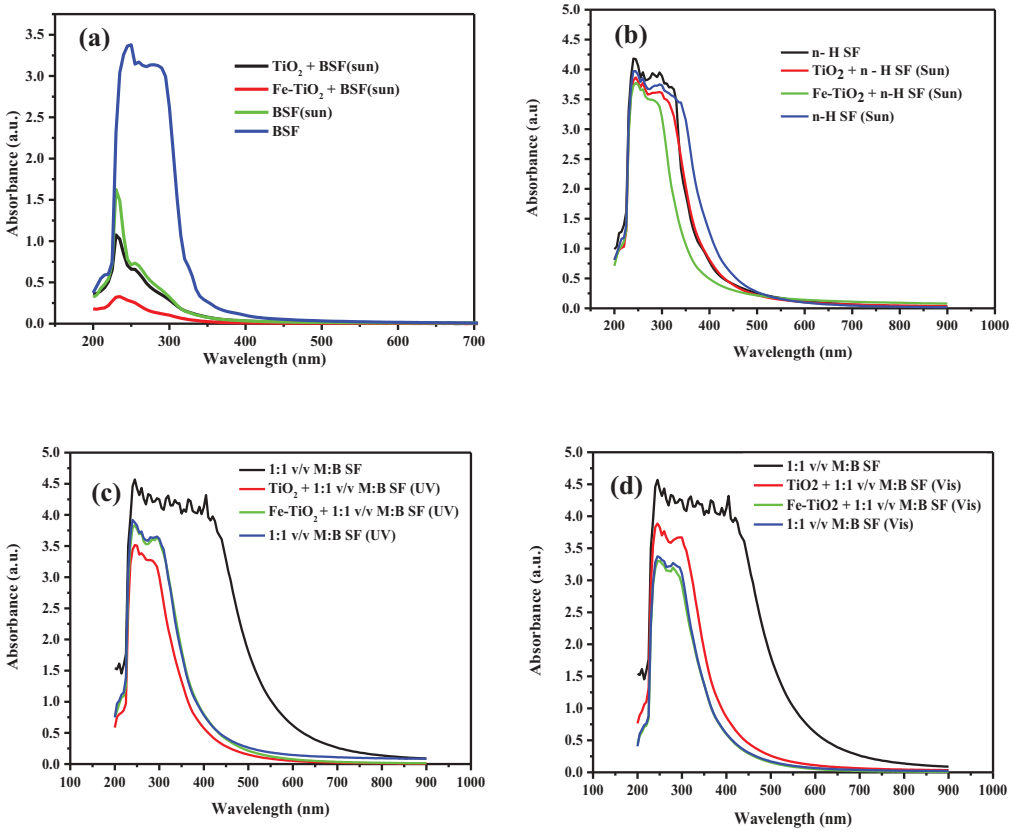

Figure 12. UV-vis Spectrum for undegraded and photodegraded (a) Benzene soluble crude oil fraction (B SF) under sunlight (Sun) irradiation, (b) n-hexane soluble crude oil fraction (n-H SF) under sunlight t(Sun) irradiation, (c) Methanol-Benzene soluble crude oil fraction (1:1 v/v M:B SF) under UV light irradiation and (d) Methanol-Benzene soluble crude oil fraction (1:1 v/v M:B SF) under visible (Vis) light irradiation.

of certain compounds from the benzene soluble fraction after photodegradation. The compounds that disappeared are presented in Table 2. The following compounds were also identified but were eluted at different retention times; hexadecane, nonadecane, and dodecane 2,6,10 trimethyl. These compounds were either undegraded or more of it were formed after sunlight irradiation. It was observed that tetradecane which was eluted at the same retention time for both the undegraded benzene soluble fraction and the TiO_2 photodegraded benzene soluble fraction had % areas of ca. 3.1 and ~1.1, respectively, which confirms that tetradecane diminished in concentration (ca. 66% degradation).

3.5.3.2. GC-MS analysis of the methanol-benzene soluble crude oil fraction after photocatalysis. Figure 14(a-c) is the GC-MS chromatogram obtained from the photodegradation of the Methanol-benzene soluble fraction of the crude oil using TiO_2 and Fe-TiO_2 photocatalysts under sunlight irradiation. Figuress 14(b,c) show that after the photodegradation, the UCM's were resolved when compared to Figure 14(a) that has a hump of UCM's ah higher retention times. There is also the formation of new peaks at the lower retention times in Figure 14(b,c) than in Figure 14(a). All these are evident of photodegradation of the methanol-benzene soluble fraction (Abdulkadir et al., 2016; Ali & Bukhari, 1989). Comparing Figuress 14(b,c), it can be observed that Fe-TiO_2 was very efficient in degrading the methanol-benzene soluble fraction. Figuress 14(b) revealed the formation of more new peaks than the fraction degraded by TiO_2 (Figure 14(c)). This also confirms that the Fe-TiO_2 is more efficient than TiO_2 in degrading the methanol-benzene soluble fraction of the crude oil under sunlight irradiation. This is evident also in the FTIR and UV-Vis spectra presented in Figures 11 and 12, respectively.

The Fe-TiO_2 and TiO_2 were able to resolve a lot of the UCM's in the undegraded methanol-benzene soluble fraction after sunlight irradiation. This also confirmed the photodegradation of the methanol-benzene soluble fraction by the Fe-TiO_2 and the TiO_2. Fe-TiO_2 was better at resolving the UCM's in the undegraded fraction than the TiO_2. Fe-TiO_2 photocatalyst eluted some compounds at a lower retention time of 6.070 s as compared to that of the TiO_2 at 7.745 s. Again, it can be

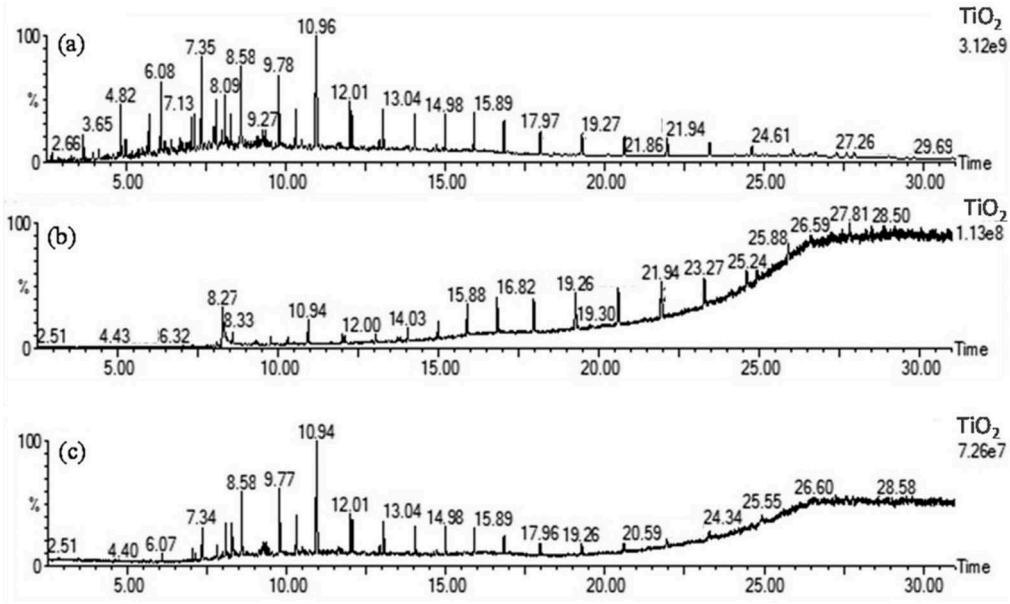

Figure 13. GC/MS chromatogram for Benzene Soluble crude oil fraction (a) undegraded, (b) degraded using Fe-TiO_2 under sunlight irradiation and (c) degraded using TiO_2 under sunlight irradiation.

Table 2. Compounds that disappeared with the Fe-TiO_2 photodegradation of the benzene soluble fraction under sunlight irradiation

#	Retention Time (RT)	Name of Compound
1	4.819	Dodecane
2	5.710	Dodecane—4,6—dimethyl
3	6.080	Tridecane
4	6.400	Naphthalene—1- methyl
5	7.030	Dodecane—2,6,10—trimethyl
6	7.130	Decahydro—4,4,8,9,10 penta methyl naphthalene
7	7.345	Tetradecane
8	7.745	Naphthalene 1,4 dimethyl
9	7.800	Decahydro—4,4,8,9,10 penta methyl naphthalene
10	7.996	Naphthalene 1,3 dimethyl
11	8.091	Heptadecane 2,6,10,14 trimethyl

inferred from the above deductions that Fe-TiO_2 is better at photodegrading the crude oil fraction than TiO_2.

3.5.3.3. GC/MS analysis of the N-Hexane soluble crude oil fraction after photocatalysis. Unidentified complex mixtures (UCM's) after sunlight irradiation of the n-hexane soluble fraction with the Fe-TiO_2 and TiO_2 photocatalysts were observed indicating degradation of the n-hexane soluble fraction. New compounds were also formed when Fe-TiO_2 photocatalyst was used for the photodegradation. These new compounds were different from the ones identified in the undegraded fraction and are presented in Table 5. The compounds that disappeared after photocatalytic degradation of the n-hexane soluble fraction by Fe-TiO_2 photocatalysts are presented in Table 4. The GC-MS chromatogram obtained from the photodegraded n-hexane soluble fraction using TiO_2 and Fe-TiO_2 are

Table 3. Compounds formed with Fe-TiO_2 photodegradation of the benzene soluble fraction under sunlight irradiation

#	Retention Time (RT)	Name of Compound
1	8.266	1—Chloroundecane
2	10.937	Heptadecane 2,6, 10, 14 tetramethyl
3	14.028	Heptadecane 9—hexyl
4	14.973	Octadecane 3- ethyl-5-2 ethylbutyl
5	15.884	Heptacosane
6	16.819	Heptacosane
7	17.960	Tetratetracontane
8	19.260	Heptacosane
9	20.596	Tetratetracontane
10	21.936	Tetratetracontane
11	23.272	Tetrapentacontane-1,54-dibromo
12	23.457	Unidentified Complex Mixtures (UCM's)
13	24.592	Pentatriacontane

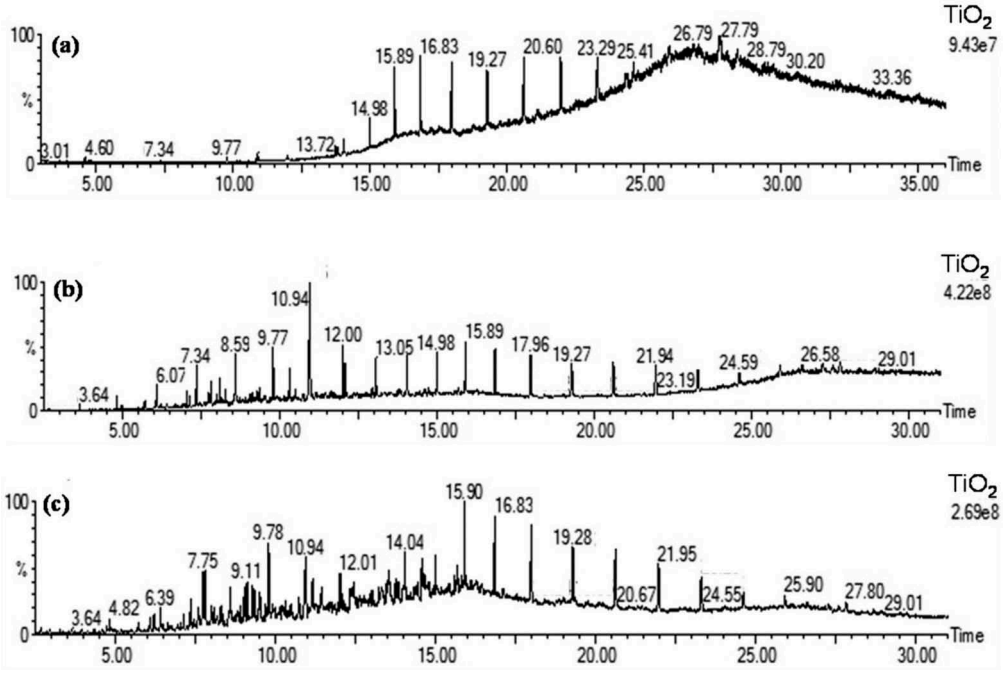

Figure 14. GC/MS chromatogram for Methanol-Benzene Soluble crude oil fraction (a) undegraded, (b) degraded using Fe-TiO_2 under sunlight irradiation and (c) degraded using TiO_2 under sunlight irradiation.

presented in Figure 15(a-c). Comparing Figuress 15(a,b) revealed the disappearance of several peaks and the appearance of a hump of unresolved complex mixtures (UCM's) after photocatalysis. The appearance of UCM's is evident of severe photodegradation of the n-hexane soluble fraction by the Fe-TiO_2. Again, comparing Figure 15(c) to that of Figure 15(a), the following were observed; new peaks were formed, some peaks were missing and some UCM's were also formed after the photocatalysis. Again, the formation of UCM's confirms that photodegradation of the crude oil fraction occurred (Abdulkadir et al., 2016; Ali & Bukhari, 1989). Comparing Figuress 15(b,c), it can be observed that Fe-TiO_2 degraded more of the n-hexane soluble fraction, showing more diminished

concentration of existing compounds, missing of known compounds and UCM's peaks which indicate severe degradation than the TiO_2. This observation is again evident in the FTIR and UV-Vis spectra presented in Figures 11 and 12, respectively.

The results showed that indeed TiO_2 and Fe-TiO_2 have the potential to photodegrade benzene, n-hexane and methanol-benzene soluble fractions in crude oil. The photodegradation resulted in the diminishing of the concentration of existing compounds, formation of new compounds and the disappearance of existing compounds. The Fe-TiO_2 out-performed the TiO_2 under sunlight and visible light irradiation due to the shift in the band gap of the TiO_2 from ~3.12 eV to ~2.9 eV for the Fe-TiO_2 and the enhanced absorption in the visible light region as observed from the DRS results. This shift made the Fe-TiO_2 active in the visible light region. The doping of the TiO_2 was done using $FeCl_3$. After the generation of the electron-hole pair upon irradiating Fe-TiO_2 with a light source, the Fe^{3+} acted as electron and hole

Table 4. Compounds that disappeared with Fe-TiO_2 photodegradation of the n-hexane soluble fraction under sunlight irradiation

#	Retention Time (RT)	Name of Compound
1	3.644	Undecane
2	4.819	Dodecane
3	4.969	1-Octanol-2-butyl
4	5.710	Dodecane 4,6 dimethyl
5	6.075	Tridecane
6	6.190	Benzocycloheptatriene
7	7.030	Dodecane 2,6,10 trimethyl
8	7.125	Dodecane 2,6,10 trimethyl
9	7.345	Decahydro-4,4,8,9,10 pentamethylnaphthalene
10	7.745	Tetradecane
11	7.800	Naphthalene 1,8-dimethyl
12	8.091	Decahydro-4,4,8,9,10 pentamethylnaphthalene
13	8.271	Dodecane 2,6,10 trimethyl
14	8.856	Decahydro-4,4,8,9,10 pentamethylnaphthalene

Table 5. Compounds formed with Fe-TiO_2 photodegradation of the n-hexane soluble fraction under sunlight irradiation

#	Retention Time (RT)	Name of compound
1	9.766	Nonadecane
2	10.902	Tert-Hexadecanethiol
3	10.937	Butane 2,2 dimethyl
4	13.738	Octadecanol 2-bromo
5	13.828	2-Nonadecanone 2,4 dimitrophenylhydrazine
6	14.028	Nonadecane
7	14.978	Nonadecane
8	15.899	Heneicosane
9	16.824	Hexacosane
10	17.965	Heptacosane
11	18.770	UCM's
12	19.260	Eicosane 2-methyl
14	20.591	Octadecane 3-ethyl-5-(2-ethylbutyl-)

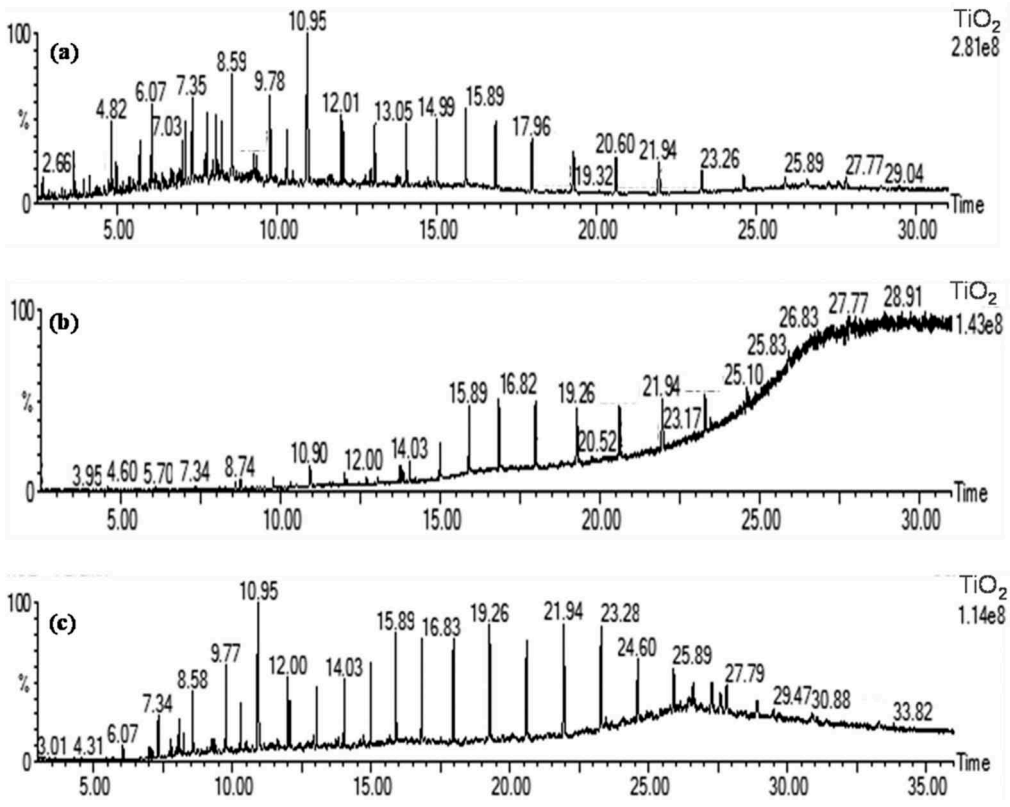

Figure 15. GC/MS chromatogram for n-Hexane Soluble crude oil fraction (a) undegraded, (b) degraded using Fe-TiO_2 under sunlight irradiation and (c) degraded using TiO_2 under sunlight irradiation.

trapping sites. The F^{3+} may either be oxidised to Fe^{4+} (Fe^{4+} is less stable than Fe^{3+}) or reduced to Fe^{2+} by the photogenerated holes or electrons, respectively. The trapping of electrons and holes by Fe^{3+} may reduce the electron-hole recombination and enhanced the photocatalysis efficiency. Also, the trapped electrons may be released back to form stable Fe^{3+} ions and result in the formation of hydroxyl radicals which may be utilized to degrade crude oil fractions (Sood et al., 2015). In addition, electrons trapped by the Fe^{3+} may be transferred to Ti^{4+} since the Ti^{3+}/Ti^{4+} energy level lies close to the energy level of Fe^{2+}/Fe^{3+} (Nyankson, Agyei-Tuffour, Adjasoo et al., 2019; Zhu et al., 2004). The smaller crystallite size of Fe-TiO_2 when compared to that of TiO_2 is also responsible for the enhanced photocatalytic activity of Fe-TiO_2.

The photodegradation of the crude oil fractions can be attributed to the generation of reactive oxygen species which in turn attacked the various compounds present in each fraction degrading them into new products. The enhanced photodegradation of the benzene soluble crude oil fraction can be attributed to their relatively higher aqueous solubility which enhanced the proximity between the benzene soluble fraction components, the photocatalyst and the reactive oxygen species generated through the photocatalysis. The results from this study showed the potential role that Fe-TiO_2 can play in visible light photodegradation of crude oil. This suggests that, photo remediation can be used as a stand-alone oil spill remediation strategy or as an add-on oil spill remediation step to enhance the degradation of water dissolvable components in crude oil. Since the photocatalysis degraded the benzene soluble fraction, which is less susceptible to biodegradation, an efficient oil spill remediation technology can be developed by combining photocatalysis and chemical dispersant application. This will enhance the removal of water-soluble components in crude oil from oceans/sea after oil spillage and as a result, reduce the threats posed by water-soluble components to aquatic species after oil spillages. Since weathered crude oil is difficult to remediate, for large scale oil spills, large amount of the photocatalysts should be readily available for application. This will be possible if the photocatalysts are synthesized in large volumes and correctly stored so that they can be used when the need arises. The storage should be done to avoid oxidation of the Fe since

oxidation of the Fe may reduce the alter the potency of the photocatalyst. In addition, since the ocean current and wave height, and the weather may influence the photocatalytic efficiency, the effect of these parameters on the photoremediation should be investigated using simulated ocean current and wave height and large-scale petroleum oil mixture. In addition, for large-scale oil spills, large amount of the photocatalysts will be required hence toxicological studies of the Fe-TiO_2 photocatalyst should be done to examine their effect on aquatic species and clean-up workers.

4. Conclusions

TiO_2 and Fe-TiO_2 were successfully synthesized by mild hydrothermal method and subsequently characterized using XRD, UV-Vis, DRS, EDX, SEM, FTIR, TGA and DSC. The results from these analyses confirmed the formation of pure anatase phase of TiO_2 and Fe-TiO_2. The optical bandgaps were estimated to be ~3.12 eV and ~2.9 eV for TiO_2 and Fe-TiO_2, respectively. This implies that while TiO_2 is active in the UV region of the electromagnetic spectrum, Fe-TiO_2 is active in both the UV and visible light region of the electromagnetic spectrum. The crystallite sizes computed using the Debye Scherrer's equation were respectively, ca. 4.1 ± 0.23 nm and ~ca. 3.85 ± 0.22 nm for the synthesized TiO_2 and Fe-TiO_2. SEM images depicted the formation of chunky uneven particles for both the TiO_2 and Fe-TiO_2 and this was attributed to the grinding of the particles after drying. The TGA/DSC results showed that the synthesized photocatalysts were stable even above temperature of 400°C. Crude oil was fractionated into three bulk fractions; the benzene soluble, n-hexane soluble and methanol-benzene soluble fractions and each fraction subjected to photocatalysis under UV, sunlight and visible light irradiation. It was revealed that the as-prepared TiO_2 and the Fe-TiO_2 were able to degrade the fractions of the crude oil after irradiation from the various light sources employed in this work. The Fe-TiO_2 showed a higher efficiency in the photocatalytic degradation of the fractionated crude oil samples than the TiO_2 in the presence of sunlight and visible light. This was due to the redshift in the Fe-TiO_2 by Fe^{3+} dopant. However, under UV light source, TiO_2 was more efficient than the Fe-TiO_2. It was again realized that TiO_2 and Fe-TiO_2 degraded more of the benzene soluble fraction and at a faster rate than the n-hexane and methanol-benzene soluble fractions. GC-MS analyses revealed that for each of the fractions investigated, new compounds were formed after photocatalysis. In addition, some of the compounds present in the undegraded fraction disappeared after photodegradation. Fe-TiO_2 photocatalysis is therefore more effective in degrading water-soluble fractions in crude oil under visible light irradiation. Hence combining photocatalysis with chemical dispersant application (bioremediation which is more effective in degrading water-insoluble fractions of crude oil but less effective in degrading water-soluble crude oil fractions) to develop photocatalyst-dispersant oil spill remediation system will result in complete remediation after oil spillages. The results, therefore, show the potential application of Fe-TiO_2 photocatalysis in oil spill remediation. The future study will involve developing a photocatalyst-dispersant system that is capable of remediating spilled crude oil by a combined photoremediation and bioremediation process and also examining the effect of ocean current and wave height on the photoremediation efficiency. Toxicological studies will also be conducted to such a system to examine its effect on aquatic species and clean-up workers.

Acknowledgements
This work was supported by the Cambridge-Africa Alborada Trust Fund and the CAPREx Fellowship Program.

Funding
The authors received no direct funding for this research.

Author details
Benjamin Agyei-Tuffour[1]
E-mail: bagyei-tuffour@ug.edu.gh
Selassie Gbogbo[1]
E-mail: sgbogbo2002@yahoo.co.uk
David Dodoo-Arhin[1]
E-mail: ddodoo-arhin@ug.edu.gh
Lucas N.W. Damoah[1]
E-mail: lnwdamoah@ug.edu.gh
Johnson K. Efavi[1]
E-mail: jkefavi@ug.edu.gh
Abu Yaya[1]
E-mail: ayaya@ug.edu.gh
Emmanuel Nyankson[1]
E-mail: enyankson@ug.edu.gh
[1] Department of Materials Science and Engineering, School of Engineering Sciences, University of Ghana, Legon-Accra, Ghana.

Citation information
Cite this article as: Photocatalytic degradation of fractionated crude oil: potential application in oil spill remediation, Benjamin Agyei-Tuffour, Selassie Gbogbo, David Dodoo-Arhin, Lucas N.W. Damoah, Johnson K. Efavi, Abu Yaya & Emmanuel Nyankson, *Cogent Engineering* (2020), 7: 1744944.

Cover image
Source: Author.

References

Abdulkadir, I., Uba, S., & Almustapha, M. (2016). A rapid method of crude oil analysis using FT-IR spectroscopy. *Nigerian Journal of Basic and Applied Sciences*, *24*(1), 47–55. https://doi.org/10.4314/njbas.v24i1.8

Agbe, H., Nyankson, E., Raza, N., Dodoo-Arhin, D., Chauhan, A., Osei, G., Kumar, V., & Kim, K.-H. (2019). Recent advances in photoinduced catalysis for water splitting and environmental applications. *Journal of Industrial and Engineering Chemistry*, *72*, 31–49. https://doi.org/10.1016/j.jiec.2019.01.004

Ajaj, B. M. A.-S. E. A. (2015). Urea modified TiO_2 nanoparticles prepared by Sol-Gel method to enhance the photocatalytic activity under sunlight. *Engineering and Technology Journal*, *33*(Part(B)), 1591–1598. https://www.iasj.net/iasj?func=fulltext&aId=117363

Akmaz, S., Iscan, O., Gurkaynak, M. A., & Yasar, M. (2011). The structural characterization of saturate, aromatic, resin, and asphaltene fractions of Batiraman crude oil. *Petroleum Science and Technology*, *29*(2), 160–171. https://doi.org/10.1080/10916460903330361

Ali, M. F., & Bukhari, A. Misbah-ul-Hasan. (1989). Structural characterization of Arabian heavy crude oil residue. *Fuel Science & Technology International*, *7*(8), 1179–1208. https://doi.org/10.1080/08843758908962284

Aske, N., Kallevik, H., & Sjöblom, J. (2001). Determination of saturate, aromatic, resin, and asphaltenic (SARA) components in crude oils by means of infrared and near-infrared spectroscopy. *Energy & Fuels*, *15*(5), 1304–1312. https://doi.org/10.1021/ef010088h

Ba-Abbad, M. M., Kadhum, A. A. H., Mohamad, A. B., Takriff, M. S., & Sopian, K. (2012). Synthesis and catalytic activity of TiO2 nanoparticles for photochemical oxidation of concentrated chlorophenols under direct solar radiation. *International Journal of Electrochemical Science*, *7*, 4871–4888. http://electrochemsci.org/papers/vol7/7064871.pdf

Buenrostro-Gonzalez, E., Espinosa-Peña, M., Andersen, S. I., & Lira-Galeana, C. (2001). Characterization of asphaltenes and resins from problematic Mexican crude oils. *Petroleum Science and Technology*, *19*(3–4), 299–316. https://doi.org/10.1081/LFT-100000764

Cheng, -H.-H., Chen, -S.-S., Yang, S.-Y., Liu, H.-M., & Lin, K.-S. (2018). Sol-Gel hydrothermal synthesis and visible light photocatalytic degradation performance of Fe/N codoped TiO2 catalysts. *Materials*, *11*(6), 939. https://doi.org/10.3390/ma11060939

Chong, M. N., Jin, B., Chow, C. W., & Saint, C. (2010). Recent developments in photocatalytic water treatment technology: A review. *Water Research*, *44*(10), 2997–3027. https://doi.org/10.1016/j.watres.2010.02.039

Coto, M., Divitini, G., Dey, A., Krishnamurthy, S., Ullah, N., Ducati, C., & Kumar, R. V. (2017). Tuning the properties of a black TiO2-Ag visible light photocatalyst produced by a rapid one-pot chemical reduction. *Materials Today Chemistry*, *4*, 142–149. https://doi.org/10.1016/j.mtchem.2017.03.002

Deng, L., Wang, S., Liu, D., Zhu, B., Huang, W., Wu, S., Zhang, S., Cheng, -H.-H., Chen, -S.-S., Yang, S.-Y., Liu, H.-M., & Lin, K.-S. (2009). Synthesis, characterization of Fe-doped TiO 2 nanotubes with high photocatalytic activity. *Catalysis Letters*, *129*(3–4), 513–518. https://doi.org/10.1007/s10562-008-9834-5

Dodoo-Arhin, D., Buabeng, F. P., Mwabora, J. M., Amaniampong, P. N., Agbe, H., Nyankson, E., Obada, D. O., & Asiedu, N. Y. (2018). The effect of titanium dioxide synthesis technique and its photocatalytic degradation of organic dye pollutants. *Heliyon*, *4*(7), e00681. https://doi.org/10.1016/j.heliyon.2018.e00681

Dong, D., Li, P., Li, X., Xu, C., Gong, D., Zhang, Y., Zhao, Q., & Li, P. (2010). Photocatalytic degradation of phenanthrene and pyrene on soil surfaces in the presence of nanometer rutile TiO2 under UV-irradiation. *Chemical Engineering Journal*, *158*(3), 378–383. https://doi.org/10.1016/j.cej.2009.12.046

Douglas, F. (2004). Gc/ms analysis. *Scientific Testimony-An Online Journal*. Accessed in 2019. http://www.scientific.org/tutorials/articles/gcms.html

Efavi, J. K., Nyankson, E., Yaya, A., & Agyei-Tuffour, B. (2017). Effect of magnesium and sodium salts on the interfacial characteristics of soybean lecithin dispersants. *Industrial & Engineering Chemistry Research*, *56*(44), 12608–12620. https://doi.org/10.1021/acs.iecr.7b02862

Etkin, D. S. (2001). Analysis of oil spill trends in the United States and worldwide. in *International oil spill conference, 2,*1291–1300. American Petroleum Institute.

Fàbrega, C., Andreu, T., Cabot, A., & Morante, J. R. (2010). Location and catalytic role of iron species in TiO2: Fe photocatalysts: An EPR study. *Journal of Photochemistry and Photobiology A: Chemistry*, *211*(2–3), 170–175. https://doi.org/10.1016/j.jphotochem.2010.03.003

Fujishima, A., Rao, T. N., & Tryk, D. A. (2000). Titanium dioxide photocatalysis. *Journal of Photochemistry and Photobiology C: Photochemistry Reviews*, *1*(1), 1–21. https://doi.org/10.1016/S1389-5567(00)00002-2

Fujishima, A., & Zhang, X. (2006). Titanium dioxide photocatalysis: Present situation and future approaches. *Comptes Rendus Chimie*, *9*(5–6), 750–760. https://doi.org/10.1016/j.crci.2005.02.055

Fujishima, A., Zhang, X., & Tryk, D. A. (2007). Heterogeneous photocatalysis: From water photolysis to applications in environmental cleanup. *International Journal of Hydrogen Energy*, *32*(14), 2664–2672. https://doi.org/10.1016/j.ijhydene.2006.09.009

García-Serrano, J., Gómez-Hernández, E., Ocampo-Fernández, M., & Pal, U. (2009). Effect of Ag doping on the crystallization and phase transition of TiO2 nanoparticles. *Current Applied Physics*, *9*(5), 1097–1105. https://doi.org/10.1016/j.cap.2008.12.008

Gaya, U. I., & Abdullah, A. H. (2008). Heterogeneous photocatalytic degradation of organic contaminants over titanium dioxide: A review of fundamentals, progress and problems. *Journal of Photochemistry and Photobiology C: Photochemistry Reviews*, *9*(1), 1–12. https://doi.org/10.1016/j.jphotochemrev.2007.12.003

Ghana, T. O. *TEN Field*. 2018. Tullow Ghana. [Retrieved February 15, 2019, from] https://www.tullowoil.com/operations/west-africa/ghana/ten-field.

Herrmann, J.-M. (1999). Heterogeneous photocatalysis: Fundamentals and applications to the removal of various types of aqueous pollutants. *Catalysis Today*, *53*(1), 115–129. https://doi.org/10.1016/S0920-5861(99)00107-8

Hoffmann, M. R., Martin, S. T., Choi, W., & Bahnemann, D. W. (1995). Environmental applications of semiconductor photocatalysis. *Chemical Reviews*, *95*(1), 69–96. https://doi.org/10.1021/cr00033a004

Hu, M., Fang, M., Tang, C., Yang, T., Huang, Z., Liu, Y., Wu, X., & Min, X. (2013). The effects of atmosphere and calcined temperature on photocatalytic activity of TiO 2 nanofibers prepared by electrospinning. *Nanoscale Research Letters*, *8*(1), 548. https://doi.org/10.1186/1556-276X-8-548

Huang, F., Yan, A., & Zhao, H. (2016). Influences of doping on photocatalytic properties of TiO2 photocatalyst. In Wenbin Cao (Ed.), *Semiconductor photocatalysis-materials, mechanisms and applications*. InTech. 31–80.

Jing, L., Xu, Z., Sun, X., Shang, J., & Cai, W. (2001). The surface properties and photocatalytic activities of ZnO ultrafine particles. *Applied Surface Science*, *180* (3–4), 308–314. https://doi.org/10.1016/S0169-4332(01)00365-8

Kim, T.-H., Rodríguez-González, V., Gyawali, G., Cho, S.-H., Sekino, T., & Lee, S.-W. (2013). Synthesis of solar light responsive Fe, N co-doped TiO2 photocatalyst by sonochemical method. *Catalysis Today*, *212*, 75–80. https://doi.org/10.1016/j.cattod.2012.09.014

Kubelka, P., & Munk, F. (1931). An article on optics of paint layers. *Z. Technical Physics*, *12*, 593–601. http://opticalbioimaging.sbu.ac.ir/wpcontent/uploads/2015/10/kubelka_munk.pdf

Lee, R. F., & Ryan, C. (1983). Microbial and photochemical degradation of polycyclic aromatic hydrocarbons in estuarine waters and sediments. *Canadian Journal of Fisheries and Aquatic Sciences*, *40*(S2), s86–s94. https://doi.org/10.1139/f83-314

Lehr, W. J. (2001). Review of modeling procedures for oil spill weathering behavior. *Advances in Ecological Sciences*, *9*, 51–90. http://citeseerx.ist.psu.edu/viewdoc/download?doi=10.1.1.226.484&rep=rep1&type=pdf

Lu, B., Ma, N., Wang, Y., Qiu, Y., Hu, H., Zhao, J., Liang, D., Xu, S., Li, X., Zhu, Z., & Cui, C. (2015). Visible-light-driven TiO2/Ag3PO4/GO heterostructure photocatalyst with dual-channel for photo-generated charges separation. *Journal of Alloys and Compounds*, *630*, 163–171. https://doi.org/10.1016/j.jallcom.2015.01.008

Mardare, D., Tasca, M., Delibas, M., & Rusu, G. I. (2000). On the structural properties and optical transmittance of TiO2 rf sputtered thin films. *Applied Surface Science*, *156*(1–4), 200–206. https://doi.org/10.1016/S0169-4332(99)00508-5

Martin, D. J., Liu, G., Moniz, S. J. A., Bi, Y., Beale, A. M., Ye, J., & Tang, J. (2015). Efficient visible driven photocatalyst, silver phosphate: Performance, understanding and perspective. *Chemical Society Reviews*, *44*(21), 7808–7828. https://doi.org/10.1039/C5CS00380F

Meng, H., Wang, B., Liu, S., Jiang, R., & Long, H. (2013). Hydrothermal preparation, characterization and photocatalytic activity of TiO2/Fe–TiO2 composite catalysts. *Ceramics International*, *39*(5), 5785–5793. https://doi.org/10.1016/j.ceramint.2012.12.098

Mills, A., & Le Hunte, S. (1997). An overview of semiconductor photocatalysis. *Journal of Photochemistry and Photobiology A: Chemistry*, *108*(1), 1–35. https://doi.org/10.1016/S1010-6030(97)00118-4

Morales, A. E., Mora, E. S., & Pal, U. (2007). Use of diffuse reflectance spectroscopy for optical characterization of un-supported nanostructures. *Revista mexicana de física*, *53*(5), 18–22. https://www.redalyc.org/pdf/570/57028299004.pdf

Murphy, A., Barnes, P., Randeniya, L., Plumb, I., Grey, I., Horne, M., & Glasscock, J. (2006). Efficiency of solar water splitting using semiconductor electrodes. *International Journal of Hydrogen Energy*, *31*(14), 1999–2017. https://doi.org/10.1016/j.ijhydene.2006.01.014

Nasiri, E. F., Kebria, D. Y., & Qaderi, F. (2018). An experimental study on the simultaneous phenol and chromium removal from water using titanium dioxide photocatalyst. *Civil Engineering Journal*, *1*(1), 585–593. https://pdfs.semanticscholar.org/0311/18f062759c44236e9dde0cb827e54433a5cf.pdf

Nyankson, E., *Smart Dispersant Formulations for Reduced Environmental Impact of Crude Oil Spills*, 2015. Auburn University

Nyankson, E., Agyei-Tuffour, B., Adjasoo, J., Ebenezer, A., Dodoo-Arhin, D., Yaya, A., Mensah, B., & Efavi, J. K. (2019). Synthesis and application of Fe-doped TiO2-halloysite nanotubes composite and their potential application in water treatment. *Advances in Materials Science and Engineering*, *2019*, 1–15. https://doi.org/10.1155/2019/4270310

Nyankson, E., Agyei-Tuffour, B., Annan, E., Yaya, A., Mensah, B., Onwona-Agyeman, B., Amedalor, R., Kwaku-Frimpong, B., & Efavi, J. K. (2019). Ag2CO3-halloysite nanotubes composite with enhanced removal efficiency for water soluble dyes. *Heliyon*, *5*(6), e01969. https://doi.org/10.1016/j.heliyon.2019.e01969

Nyankson, E., DeCuir, M. J., & Gupta, R. B. (2015). Soybean lecithin as a dispersant for crude oil spills. *ACS Sustainable Chemistry & Engineering*, *3*(5), 920–931. https://doi.org/10.1021/acssuschemeng.5b00027

Nyankson, E., Demir, M., Gonen, M., & Gupta, R. B. (2016). Interfacially active hydroxylated soybean lecithin dispersant for crude oil spill remediation. *ACS Sustainable Chemistry & Engineering*, *4*(4), 2056–2067. https://doi.org/10.1021/acssuschemeng.5b01403

Nyankson, E., & Kumar, R. (2019). Removal of water-soluble dyes and pharmaceutical wastes by combining the photocatalytic properties of Ag3PO4 with the adsorption properties of halloysite nanotubes. *Materials Today Advances*, *4*, 100025. https://doi.org/10.1016/j.mtadv.2019.100025

Nyankson, E., Ober, C. A., DeCuir, M. J., & Gupta, R. B. (2014). Comparison of the effectiveness of solid and solubilized dioctyl sodium sulfosuccinate (DOSS) on oil dispersion using the baffled flask test, for crude oil spill applications. *Industrial & Engineering Chemistry Research*, *53*(29), 11862–11872. https://doi.org/10.1021/ie5017249

Nyankson, E., Olasehinde, O., John, V. T., & Gupta, R. B. (2015). Surfactant-loaded halloysite clay nanotube dispersants for crude oil spill remediation. *Industrial & Engineering Chemistry Research*, *54*(38), 9328–9341. https://doi.org/10.1021/acs.iecr.5b02032

Nyankson, E., Rodene, D., & Gupta, R. B. (2016). Advancements in crude oil spill remediation research after the Deepwater Horizon oil spill. *Water, Air, & Soil Pollution*, *227*(1), 29. https://doi.org/10.1007/s11270-015-2727-5

Owoseni, O., Nyankson, E., Zhang, Y., Adams, D. J., He, J., Spinu, L., McPherson, G. L., Bose, A., Gupta, R. B., & John, V. T. (2016). Interfacial adsorption and surfactant release characteristics of magnetically functionalized halloysite nanotubes for responsive emulsions. *Journal of Colloid and Interface Science*, *463*, 288–298. https://doi.org/10.1016/j.jcis.2015.10.064

Owoseni, O., Nyankson, E., Zhang, Y., Adams, S. J., He, J., McPherson, G. L., Bose, A., Gupta, R. B., & John, V. T. (2014). Release of surfactant cargo from interfacially-active halloysite clay nanotubes for oil spill remediation. *Langmuir*, *30*(45), 13533–13541. https://doi.org/10.1021/la503687b

Peralta-Martinez, M., Vázquez-Ramírez, R., Blass-Amador, G., & Palacios-Lozano, E. M. (2008). Determination of functional groups in Mexican vacuum residua.

Petroleum Science and Technology, *26*(1), 91–100. https://doi.org/10.1080/10916460600705816

Plata, D. L., Sharpless, C. M., & Reddy, C. M. (2008). Photochemical degradation of polycyclic aromatic hydrocarbons in oil films. *Environmental Science & Technology*, *42*(7), 2432–2438. https://doi.org/10.1021/es702384f

Santos, R. D. S., Faria, G. A., Giles, C., Leite, C. A. P., Barbosa, H. D. S., Arruda, M. A. Z., & Longo, C. (2012). Iron insertion and hematite segregation on Fe-doped TiO2 nanoparticles obtained from sol–gel and hydrothermal methods. *ACS Applied Materials & Interfaces*, 4 (10), 5555–5561. https://doi.org/10.1021/am301444k

Sood, S., Umar, A., Mehta, S. K., & Kansal, S. K. (2015). Highly effective Fe-doped TiO2 nanoparticles photocatalysts for visible-light driven photocatalytic degradation of toxic organic compounds. *Journal of Colloid and Interface Science*, *450*, 213–223. https://doi.org/10.1016/j.jcis.2015.03.018

Tang, A., Deng, Y., Jin, J., & Yang, H. (2012). ZnFe2O4-TiO2 nanoparticles within mesoporous MCM-41. *The Scientific World Journal*, *2012*, 1–8. https://doi.org/10.1100/2012/480527

Wang, C.-Y., Bahnemann, D. W., & Dohrmann, J. K. (2000). A novel preparation of iron-doped TiO2 nanoparticles with enhanced photocatalytic activity. *Chemical Communications*, 16, 1539–1540. https://doi.org/10.1039/b002988m

Wang, J., Sun, W., Zhang, Z., Jiang, Z., Wang, X., Xu, R., Li, R., & Zhang, X. (2008). Preparation of Fe-doped mixed crystal TiO2 catalyst and investigation of its sonocatalytic activity during degradation of azo fuchsine under ultrasonic irradiation. *Journal of Colloid and Interface Science*, *320*(1), 202–209. https://doi.org/10.1016/j.jcis.2007.12.013

Xu, Z., Shang, J., Liu, C., Kang, C., Guo, H., & Du, Y. (1999). The preparation and characterization of TiO2 ultrafine particles. *Materials Science and Engineering: B*, *63* (3), 211–214. https://doi.org/10.1016/S0921-5107(99)00084-7

Yoon, C., & Cocke, D. L. (1986). Potential of amorphous materials as catalysts. *Journal of Non-crystalline Solids*, *79*(3), 217–245. https://doi.org/10.1016/0022-3093(86)90224-3

Yu, J., Zhao, X., & Zhao, Q. (2000). Effect of surface structure on photocatalytic activity of TiO2 thin films prepared by sol-gel method. *Thin Solid Films*, *379* (1–2), 7–14. https://doi.org/10.1016/S0040-6090(00)01542-X

Zhou, J., Zhu, B., Wang, L., Li, Y., & Qiao, Q. (2017). Enhanced photocatalytic activity of Fe-doped TiO2 coated on N-doped activated carbon composites for photocatalytic degradation of dyeing wastewater. *In AIP Conference Proceedings*, 1890(1), 020009. AIP Publishing LLC.

Zhu, J., Zheng, W., He, B., Zhang, J., & Anpo, M. (2004). Characterization of Fe–TiO2 photocatalysts synthesized by hydrothermal method and their photocatalytic reactivity for photodegradation of XRG dye diluted in water. *Journal of Molecular Catalysis A: Chemical*, *216*(1), 35–43. https://doi.org/10.1016/j.molcata.2004.01.008

Ziervogel, K., McKay, L., Rhodes, B., Osburn, C. L., Dickson-Brown, J., Arnosti, C., & Teske, A. (2012). Microbial activities and dissolved organic matter dynamics in oil-contaminated surface seawater from the Deepwater Horizon oil spill site. *PloS One*, *7*(4), e34816. https://doi.org/10.1371/journal.pone.0034816

Cogent Engineering **(ISSN: 2331-1916) is published by Cogent OA, part of Taylor & Francis Group.**